Solid-Hexatic-Liquid Phases in Two-Dimensional Charge-Density Waves

Hongjie Dai and Charles M. Lieber
Harvard University, 12 Oxford Street, Cambridge, Massachusetts 02138
(Received 16 June 1992)

The structural order of the two-dimensional (2D) charge-density-wave (CDW) phase in $Nb_xTa_{1-x}S_2$ materials has been determined as a function of impurity concentration from the quantitative analysis of scanning tunneling microscopy images. We show that the CDW phase evolves through crystalline, hexatic glass, and liquidlike states as the impurity concentration in the lattice increases to $x=0.10$. These results address systematically the structural manifestations of quenched disorder in 2D systems.

PACS numbers: 71.45.Lr, 61.16.Di, 64.70.Kb, 74.60.Ge

The phenomenon of two-dimensional (2D) melting has been the focus of considerable effort for a number of years [1-9]. For an equilibrium melting transition Halperin and Nelson showed that a 2D solid can melt in a continuous transition through a hexatic state that is characterized by long-range orientational order and exponentially decaying positional order [2]. More recently, there has been much interest and controversy concerning the proposed hexatic state of the flux-line lattice (FLL) in the copper-oxide superconductors [10-14]. Murray and co-workers suggested from the analysis of real-space magnetic decoration images that at low temperatures the ordered state of the FLL is a hexatic glass [10]. The observation of a hexatic versus a crystalline Abrikosov lattice is presumably due to pinning of the FLL by impurities and/or disorder in the lattice. The implication of impurity pinning raises several more general issues. First, the theory of 2D melting is based upon thermal disorder whereas quenched disorder (a frozen impurity distribution) dominates the FLL hexatic. Since the statistical averaging differs for these two types of disorder [15] it is important to examine carefully the similarities with equilibrium theory. In addition, impurity pinning manifests itself in other important, low-dimensional systems such as charge-density waves (CDWs) [16,17]. The CDW and FLL problems are especially analogous since they can be cast in terms of the elastic properties of the lattice and a random impurity potential [17]. However, to understand the complex behavior exhibited by these systems it remains essential to develop a more detailed picture of impurity pinning.

To elucidate the role that impurity pinning and disorder play on the structure of 2D systems we have carried out a quantitative study of the relationship of impurity concentration and structural order in the 2D CDW system $Nb_xTa_{1-x}S_2$. We have used a variable-temperature scanning tunneling microscope (STM) to obtain real-space images of the incommensurate CDW superlattice for $0 \leq x \leq 0.1$, and have quantitatively characterized the topological defects, translational order, and orientational order in these images. In a preliminary study, we reported evidence for weak pinning in this system, and speculated on the existence of a hexatic state [18]. Herein, we prove that the CDW is weakly pinned in $Nb_xTa_{1-x}S_2$, and more importantly we show how the system evolves through 2D crystalline, hexatic glass, and liquidlike states as a function of impurity concentration.

Single crystals of $Nb_xTa_{1-x}S_2$ ($x=0$, 0.02, 0.04, 0.07, and 0.10) were imaged in the incommensurate state ($T=320$-380 K), using methods described previously [18,19]. The digital STM images were then analyzed using procedures outlined by Murray and co-workers [7,10]. Briefly, the CDW maxima, which we call the lattice points, were located to ± 1 pixel accuracy using standard image-analysis algorithms. These computer-generated lattices were checked interactively with the original images before proceeding with the analysis. Typically, images 30 to 90 lattice constants on edge were examined, although the maximum number of lattice sites that could be used in our calculations was 4000.

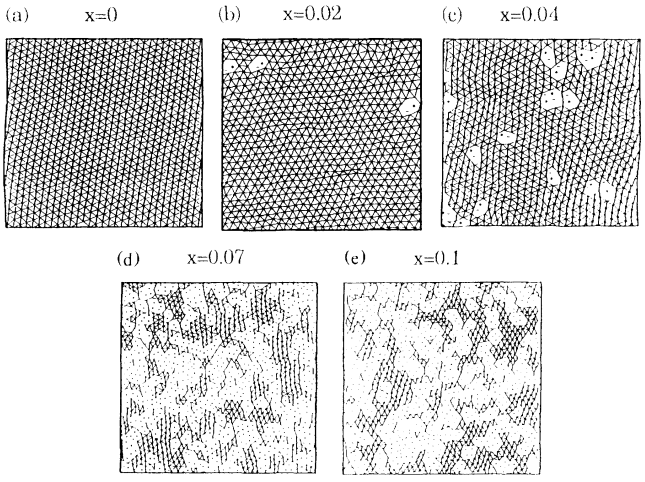

FIG. 1. Delauney triangulations of the STM images recorded on $Nb_xTa_{1-x}S_2$ crystals where (a) $x=0$, (b) $x=0.02$, (c) $x=0.04$, (d) $x=0.07$, and (e) $x=0.10$. Sixfold-coordinated sites (CDW maxima) are indicated by "bonds" to the nearest neighbors, while defect sites are highlighted without bonds. Dislocations consisting of fivefold- and sevenfold-coordinated disclination pairs are highlighted by $-$ and $+$, respectively, in (b) and (c). The coordination numbers of the extensive defect networks in (d) and (e) are not explicitly shown.

To determine the nature of the topological defects in the CDW lattice versus the impurity concentration we have carried out a Delauney triangulation of the STM images (Fig. 1) [7,20]. The triangulation uniquely defines the nearest neighbors and thus the coordination number of each CDW maxima. Fully coordinated lattice sites are indicated by six bonds to the CDW maxima, while defects are highlighted as vertices without bonds. Analyses of the images recorded on pure TaS_2 are typically free of topological defects; i.e., all lattice sites are sixfold coordinated [Fig. 1(a)]. However, for the $Nb_xTa_{1-x}S_2$ ($x>0$) materials the Delauney triangulations provide clear evidence for topological defects in the CDW lattice. At low values of Nb impurities [x(Nb) $=0.02,0.04$] we observe dislocations that typically consist of fivefold- to sevenfold-coordinated disclination pairs [Figs. 1(b) and 1(c)]. Analyses of several data sets further show that the average separation of the dislocations in the x(Nb) $=0.02$ and 0.04 images is 15 and 6.6 lattice constants, respectively. Notably, since the average separation between Nb impurities is much smaller than the corresponding dislocation separation (1.9 vs 6.6 and 3.8 vs 15) these results confirm that this system is in the weak pinning regime. As x(Nb) is increased further to 0.07 and 0.10, extensive defects networks are observed in the triangulated STM images. These extended topological defects can be assigned to dislocations and free disinclinations. There are also several qualitative conclusions that can be made from the triangulation results. First, the topological defects are spatially fixed in the lattice on the time scale of imaging (5–60 min). These data indicate that the defects do not arise from thermal fluctuations, but instead reflect the quenched impurity distribution. In addition, the observed evolution of the topological defects with increasing Nb substitution is quite similar to the behavior expected for 2D melting, via an equilibrium hexatic [2]. In our case it appears that a hexatic to liquidlike phase transition occurs between an impurity concentration of 0.04 and 0.07.

To elucidate further the structural phases as a function of impurity concentration and explore the analogy with 2D melting we have examined the structure factor, translational correlation function, and orientational correlation function. Structure factors $S(k)$ were calculated from the Fourier transform of the STM images; representative results are shown in Fig. 2. $S(k)$ for pure TaS_2 exhibits sharp sixfold symmetric peaks that broaden gradually as the impurity concentration increases to 0.04 [Figs.

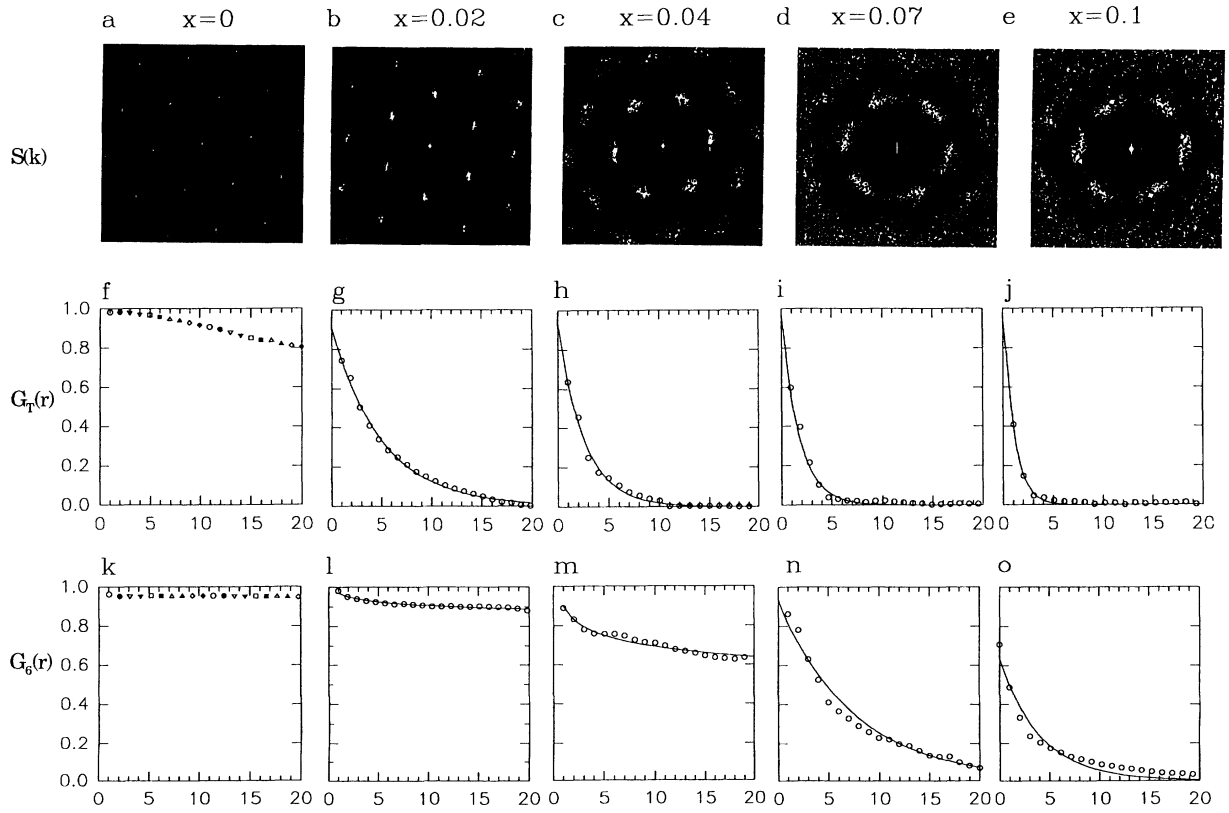

FIG. 2. (a)–(e) Structure factors; (f)–(j) translational correlation functions $GT(r)$; (k)–(o) orientational correlation functions $G_6(r)$ calculated from images of $x=0$, 0.02, 0.04, 0.07, and 0.10 $Nb_xTa_{1-x}S_2$ materials, respectively. The x axes in (f)–(o) correspond to lattice constants. The points represent the experimental data and the lines correspond to exponential [$\exp(-\xi/T)$] fits (g)–(j), (n), and (o), or power-law ($r^{-\eta}$) fits (l) and (m).

2(a)-2(c)]. For the $x(\mathrm{Nb})=0.07$ and 0.10 samples the first-order Bragg peaks have broadened to form a ring whose intensity has a sixfold modulation (Figs. 2(d) and 2(e)]. In addition, the radial width of Bragg peaks indicates that the translational correlation length is short in all of the samples that contain Nb impurities. These features are strikingly similar to the results expected for 2D melting, and thus support the idea that this CDW system evolves through a hexatic state.

We have confirmed the existence of a hexatic state and defined the structural evolution of this system by calculating the translational and orientational correlation functions $G_T(r)$ and $G_6(r)$, respectively [21]. These results are summarized in Figs. 2(f)-2(o). $G_T(r)$ and $G_6(r)$ decay very little over 20 lattice constants for the pure sample. However, all of the samples that contain Nb impurities exhibit a rapid decay of translational order. This decay in $G_T(r)$ can be fitted reasonably well by $\exp(-\xi_T/r)$, where ξ_T is the translational correlation length. The range of the ξ_T's determined from a number of images are 7-10, 3-6, 2-3, and 1-2 lattice constants for the $x(\mathrm{Nb})=0.02$, 0.04, 0.07, and 0.10 samples, respectively. In contrast, we find that the orientational correlations die out slowly for the 0.02 and 0.04 samples, but decay rapidly for $x(\mathrm{Nb})=0.07$ and 0.10. If we fit the $x(\mathrm{Nb})=0.02$, 0.04, 0.07, and 0.10 data with an exponential $[\exp(-\xi_6/r)]$ we obtain correlation lengths of $\xi_6 \approx 200$, 100, 11, and 5 lattice constants. A better fit to $G_6(r)$ for $x(\mathrm{Nb})=0.02,0.04$ is obtained, however, using an algebraic decay $r^{-\eta}$, with $\eta=0.03$ and 0.12, respectively. These results are strongly suggestive of 2D melting driven by topological defects. In this system, however, the topological defects arise from impurity pinning and not from thermal fluctuations. Investigating this analogy further we estimate that the power-law exponent η using the relation $\eta=9c/\pi$, where c is a fractional area of dislocation cores [6]. The values of η calculated in this way, 0.02 and 0.13, are in excellent agreement with the values obtained from fits to $G_6(r)$ for $x(\mathrm{Nb})=0.02,0.04$. The average dislocation spacing (ξ_D) is also similar to ξ_T, although at the smallest impurity concentration ξ_D is always larger than ξ_T.

We thus believe that our results show a detailed and rich evolution of a 2D (CDW) structure from crystalline through hexatic glass to liquidlike states as the impurity concentration in the lattice is systematically increased. We assign the intermediate state to a hexatic glass (versus equilibrium hexatic) since the impurity distributions in these materials are quenched. The intermediate hexatic may correspond to two regimes, including (1) $\xi_T < \xi_D$, the Chudnovsky hexatic [11], and (2) $\xi_T \approx \xi_D$, the Halperin-Nelson hexatic [2]. It is interesting to ask whether there are observable consequences of these novel structural phases. Measurements of the temperature-dependent resistivity show that the sharp first-order incommensurate-nearly-commensurate (IC-NC) transition in pure TaS_2 broadens significantly for $x(\mathrm{Nb})=0.02$ and 0.04 and then disappears for $x(\mathrm{Nb}) \geq 0.07$ (Fig. 3). Hence, the crystalline CDW state maps to the sharp first-order transition, the hexatic glass state can be associated with the broadened transition, and in the amorphous state the IC-NC transition is no longer observed. These results do show that there are macroscopic consequences of these structural studies.

These results also help to address the validity of theoretical models proposed to explain the hexatic glass state of the FLL lattice in copper-oxide superconductors [11-14]. The pinning problem for both CDWs and the FLL can be cast similarly in terms of the elastic properties of the CDW lattice or FLL and the random impurity potential [11,17]. In this context, Chudnovsky has shown that a hexatic glass state should be observed for the FLL in the presence of randomly distributed pinning sites [17]. Our results support this model since we have shown that the introduction of weak pinning sites leads to a hexatic glass CDW state. However, our data indicate that the hexatic glass state also includes impurity-induced dislocations. Other work has considered the effects of dislocations in weakly pinned systems [12,22]. Toner suggests that orientational order will decay exponentially if interactions between dislocations and the lattice are ignored; however, if coupling is included "apparent" long-range order will be observed. A consequence of this work is that $\xi_6 \approx \xi_T^2/a$ in the limit of weak disorder [14]. Although our results do not verify this scaling argument, we believe that orientational coupling of the sixfold CDW and crystal lattices is probably important. It will be possible to test the role of coupling further by making analogous measurements in the NC state where the coupling to the lattice is stronger, and at higher temperatures in the IC state where the coupling should be smaller.

In conclusion, we have carried out detailed quantitative analyses of the topological defects, structure factors, and

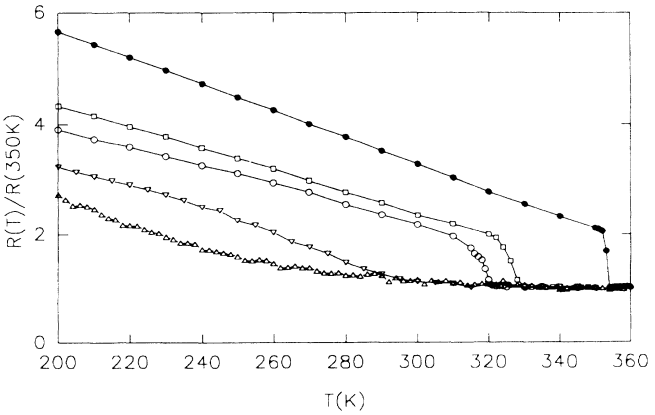

FIG. 3. Normalized resistance vs temperature curves recorded on TaS_2 (●), $Nb_{0.02}Ta_{0.98}S_2$ (□), $Nb_{0.04}Ta_{0.96}S_2$ (○), $Nb_{0.07}Ta_{0.93}S_2$ (▽), and $Nb_{0.1}Ta_{0.9}S_2$ (△).

translational and orientational correlation functions for the 2D CDW lattice in a series of impurity-doped $Nb_xTa_{1-x}S_2$ materials. These results show that the CDW lattice evolves from a crystalline state in the pure solid through a hexatic glass state to a liquidlike state as the impurity concentration in the lattice increases. These phases are driven by impurity-induced dislocations in the CDW lattice, and thus are similar to 2D melting. The importance of dislocations and coupling to the lattice will require, however, further experimental and theoretical examination. We believe that $Nb_xTa_{1-x}S_2$ will be an ideal system for future studies since the impurity concentration can be varied systematically, and since the CDW-lattice coupling can be changed significantly through variations in the temperature.

We thank D. R. Nelson for insightful discussion. C.M.L. acknowledges support of this work by the National Science Foundation and Air Force Office of Scientific Research.

[1] J. M. Kosterlitz and D. J. Thouless, J. Phys. Chem. **6**, 1181 (1973).

[2] B. I. Halperin and D. R. Nelson, Phys. Rev. Lett. **41**, 121 (1978); D. R. Nelson and B. I. Halperin, Phys. Rev. B **19**, 2457 (1979).

[3] A. P. Young, Phys. Rev. B **19**, 1855 (1979).

[4] D. R. Nelson, in *Phase Transitions and Critical Phenomena*, edited by C. Domb and J. L. Lebowitz (Academic, London, 1983), Vol. 7, p. 1.

[5] K. J. Strandburg, Rev. Mod. Phys. **60**, 161 (1988).

[6] D. R. Nelson, M. Rubinstein, and F. Spaepen, Philos. Mag. A **46**, 105 (1982).

[7] C. A. Murray, W. O. Sprenger, and R. A. Wenk, Phys. Rev. B **42**, 688 (1990).

[8] N. Greiser, G. A. Held, R. Frahm, R. L. Greene, P. M. Horn, and R. M. Suter, Phys. Rev. Lett. **59**, 1706 (1987).

[9] R. Seshadri and R. M. Westervelt, Phys. Rev. Lett. **66**, 2774 (1991).

[10] C. A. Murray, P. L. Gammel, D. J. Bishop, D. B. Mitzi, and A. Kapitulnik, Phys. Rev. Lett. **64**, 2312 (1990); D. G. Grier, C. A. Murray, C. A. Bolle, P. L. Gammel, D. J. Bishop, D. B. Mitzi, and A. Kapitulnik, Phys. Rev. Lett. **66**, 2270 (1991).

[11] E. M. Chudnovsky, Phys. Rev. B **40**, 11355 (1989); **43**, 7831 (1991).

[12] J. Toner, Phys. Rev. Lett. **66**, 2523 (1991).

[13] E. M. Chudnovsky, Phys. Rev. Lett. **67**, 1809 (1991).

[14] J. Toner, Phys. Rev. Lett. **67**, 1810 (1991).

[15] S.-K. Ma, *Modern Theory of Critical Phenomena* (Benjamin/Cummings, Reading, MA, 1976).

[16] G. Gruner, Rev. Mod. Phys. **60**, 1129 (1988).

[17] H. Fukuyama and P. A. Lee, Phys. Rev. B **17**, 535 (1978); P. A. Lee and T. M. Rice, *ibid.* **19**, 3970 (1979).

[18] H. Dai, H. Chen, and C. M. Lieber, Phys. Rev. Lett. **66**, 3183 (1991).

[19] STM images typical of those used for the analysis in this paper have been reported in the past [18]. Herein we show only the Delauney triangulations of the STM images.

[20] F. F. Preparata and M. L. Shamos, *Computational Geometry, an Introduction* (Springer-Verlag, New York, 1985).

[21] The translational correlation function, $G_T(r)$, is defined as $G_T(r)=\langle\psi_T(a)\psi_T(r)^*\rangle$, where $\psi_T(r)=\sum\exp(iG\cdot r)$ is the translational order parameter. The sum is over the three reciprocal-lattice vectors (G) determined from the structure factor. The orientational correlation function, $G_6(r)$, is defined as $G_6(r)=\langle\psi_6(0)\psi_6(r)^*\rangle$. The bond orientational order parameter is $\psi_6(r)=\sum\exp[i6\theta(r)]$, where $\theta(r)$ is an angle with respect to a fixed axis of the bond between the CDW maxima located at r and its nearest neighbor [6,10].

[22] M. C. Marchetti and D. R. Nelson, Phys. Rev. B **41**, 1910 (1990).

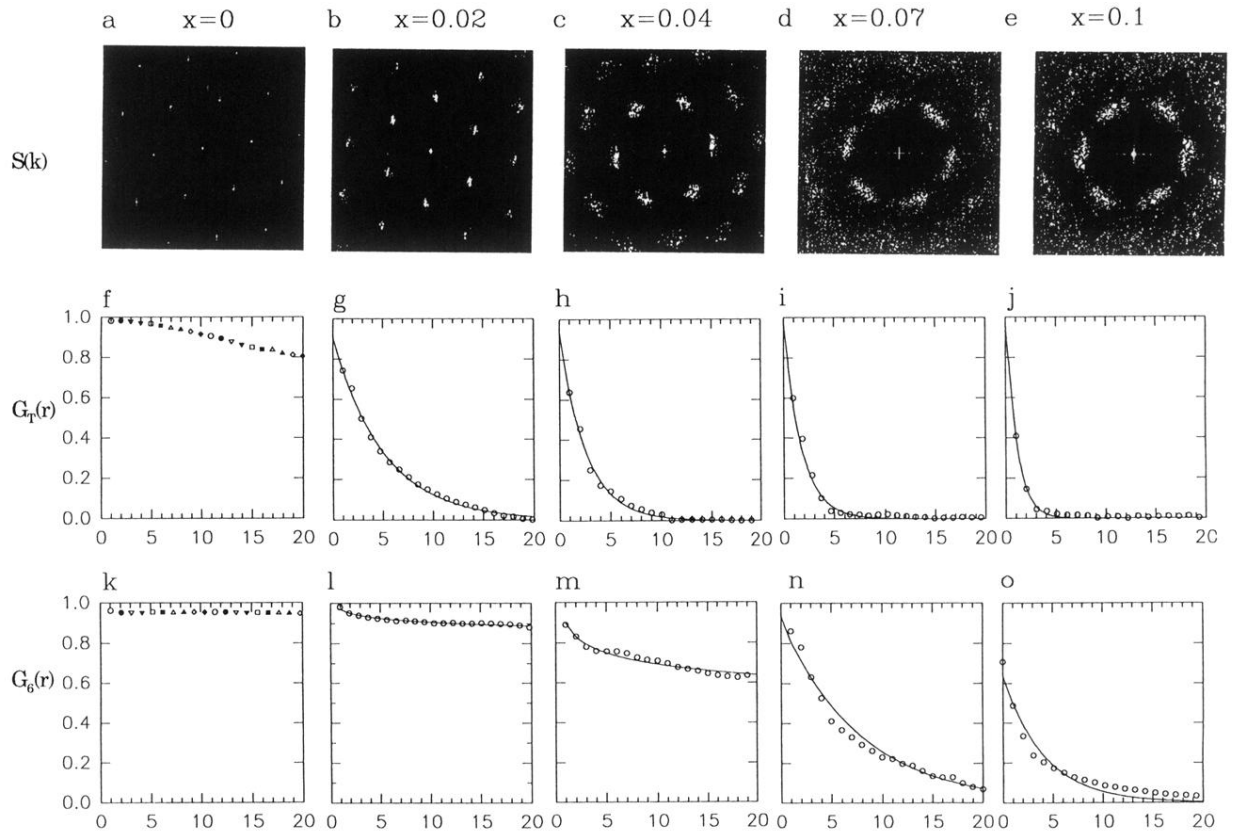

FIG. 2. (a)-(e) Structure factors; (f)-(j) translational correlation functions $GT(r)$; (k)-(o) orientational correlation functions $G_6(r)$ calculated from images of $x=0$, 0.02, 0.04, 0.07, and 0.10 $Nb_xTa_{1-x}S_2$ materials, respectively. The x axes in (f)-(o) correspond to lattice constants. The points represent the experimental data and the lines correspond to exponential $[\exp(-\xi/T)]$ fits (g)-(j), (n), and (o), or power-law ($r^{-\eta}$) fits (l) and (m).